Turkish Journal of Earth Sciences

Volume 30 | Number 5 Article 9

1-1-2021

Long-term spatiotemporal evolution of land subsidence in Konya metropolitan area (Turkey) based on multisensor SAR data

NURDAN ŞİRECİ

GÖKHAN ASLAN

ZİYADİN ÇAKIR

TÜBİTAK

Turkish Journal of Earth Sciences
http://journals.tubitak.gov.tr/earth

Research Article

Turkish J Earth Sci
(2021) 30: 681-697

doi: 10.3906/yer-2104-22

Long-term spatiotemporal evolution of land subsidence in Konya metropolitan area (Turkey) based on multisensor SAR data

Nurdan ŞİRECİ[1,*], Gökhan ASLAN[2], Ziyadin ÇAKIR[1]
[1] Department of Geological Engineering, Faculty of Mines, Istanbul Technical University, İstanbul, Turkey
[2]Natural Risk Department, BRGM—French Geological Survey, Orléans, France

Received: 27.04.2021 **Accepted/Published Online:** 10.08.2021 **Final Version:** 28.09.2021

Abstract: We have studied the spatiotemporal evolution of surface deformation in Konya city and its vicinity using advanced multitemporal synthetic aperture radar techniques with SAR data acquired by Envisat, ALOS-1, and Sentinel-1 A/B satellites between 2004 and 2020. Velocity maps and time series show that the city has been subsiding with varying rates in space and time since 2004. The pattern of deformation shows two main lobes of subsidence centered in the western and eastern sides of the city with a nondeforming north-south trending narrow zone in between. Subsidence rate increases from a few cm/yr to 11 cm/yr between 2014 and 2019. As of 2019, subsidence has slowed down dramatically, giving rise to uplift in some places. Spatiotemporal variation of subsidence and its strong correlation with change in water table level confirm the inferences that subsidence in the metropolitan area of Konya is due to over drafting of the ground water for urban needs. The decrease in subsidence rate over the last two years appears to be due to the city's residents supplying their water from recently built dams instead of aquifers beneath the city. Initial excessive groundwater extraction in agricultural areas caused ~4 m drops every year in the water table level, which, in turn, gave rise to 8 cm subsidence every year. Modeling of the subsidence shows 7.7 x 10^6 m^3/yr volume loss due to compaction of the aquifer in the Konya metropolitan area and its vicinity between 2014 and 2018.

Key words: Konya, subsidence, groundwater, InSAR, modeling

1. Introduction

Land subsidence resulting from excessive groundwater extraction is one of the major environmental problems in the developing world as cities increase in population and water use in the absence of adequate pumping regulation and enforcement (Haghshenas and Motagh, 2018). The land subsidence due to over-extraction of groundwater from aquifer systems can cause serious damages to the urban components such as motorways, buildings and underground structures in the long-term. Multiple studies have documented that many cities have undergone severe land subsidence in recent years as a result of groundwater extraction. This settlement phenomena mostly occurs when a large amount of groundwater has been extracted from unconsolidated alluvial or basin-fill aquifer system as a result ground compaction. Multiple groundwater-related land subsidence phenomena have been observed in cities in Indonesia (Du et al. 2018), Iran (Motagh et al., 2008; Khorrami et al., 2020), Italy (Peduto et al., 2015; Rosi et al., 2016), Mexico (Castellazzi et al., 2017; Figueroa-Miranda et al., 2018), the United States (Amelung et al., 1999; Bekaert et al., 2017; Riel et al., 2018), Spain (Fernandez et al., 2018) and Turkey (Aslan et al., 2019; Imamoglu et al., 2019; Orhan, 2021).

Knowledge of the spatial and temporal extents of land subsidence is necessary for developing water management programs and establishing measures to mitigate hazards associated with land settlements and infrastructure (Haghshenas and Motagh, 2018). In Turkey, land subsidence due to groundwater extraction is reported for İstanbul, Afyon and Bursa (Aslan et al., 2019; Imamoğlu et al., 2019). Land subsidence in the Konya region has long been known and documented geodetically first by Ustun et al. (2010) using GPS measurements. Establishing and measuring 6 GPS benchmarks, they found subsidence with rates reaching up to 5.2 cm/y. The maximum subsidence is found to be near the city, south of the city center. Since GPS measurements are pointwise measurements, they did not reveal a full picture of the pattern of subsidence. First, InSAR observations in the study area were made by Ustun et al. (2016) using limited amount of Envisat SAR imagery over the Karapınar region.

The ongoing subsidence in the metropolitan parts of the city is poorly known since no detail or comprehensive studies on this subsidence has been reported in the literature. Çomut et al., (2016) were the first to use InSAR technique with Sentinel-1 A/B and CosmoSky-Med images between 2014 and 2015 and report the subsidence in the metropolitan area of Konya. They found a maximum of 6 cm/yr subsidence cantered near the railway station. However, this study is based on a very short observation period, that is, 1.5 years of Sentinel data only and, hence, does not reveal the entire pattern of deformation in the city. Recently, Orhan (2021) used Sentinel-1 A/B data between October 5, 2014 and February 04, 2018 and found ground subsidence up to 7.5 cm/yr. Both Çomut et al., (2016) and Orhan (2021) used only one track, that is, ascending or descending. Other InSAR observations in the Konya plain are mostly focused around the Karapınar

*Correspondence: sireci@itu.edu.tr

region where widespread sinkhole formations are present (Üstün et al., 2015; Caló, et al., 2017; Orhan et al. 2021).

Here, we calculate time series of deformation with advanced multitemporal InSAR techniques using descending ENVISAT images between 2004 and 2010, ascending ALOS images between 2006 and 2010, and ascending and descending Sentinel-1 A/B TOPS images between 2014 and 2020 in order to reveal the spatiotemporal pattern of ground subsidence in the entire Konya city since 2004 (Figure 1). We model the surface deformation deduced from Sentinel data using elastic dislocations on triangular and rectangular surfaces. We also use groundwater level changes over the last five years where lobes of rapid subsidence are centered. The results obtained from multisensor InSAR time-series are compared with groundwater level over the last five years to understand how land subsidence evolves in response to the water table fluctuations.

2. Study area

The study area is located in the metropolitan region of Konya city in the northwest of the Konya Basin (Figure 1). Elevation of the city is approximately 1030 m on the south-western edge of the Central Anatolian Plateau (Figure 1). The Neolithic City of Çatalhöyük included in the UNESCO's World Heritage list where social developments such as the transition of humanity to settled life, the beginning of agriculture and hunting, is located in Çumra district of Konya (Figure 1).

Today, the economy of Konya is still based largely on agriculture (mostly wheat, maize and sugar beet cultivation) although it is one of the driest regions of Turkey. The annual precipitation of the basin is 329 mm (measurement years range 1929–2018, Turkish State Meteorological Service). As the city of Konya is a large closed basin, it is thought to hold about 17% of the groundwater reserve of Turkey. Total annual usable water resource in the basin is 4.3 billion m^3, and annual water consumption is around 6.5 billion m^3 with more than 90% of it being used for agricultural purposes. Thus, an annual deficit of about 2 billion m^3 exists in the water budget of the basin (WWF-Türkiye, 2014). Most of the water budget deficit in question is retrieved from groundwater, which results in rapid drop of ground water table over time making the environmental and agricultural sustainability difficult. Despite the deficit in the water, budget, alfalfa, corn, potato and sunflower, which are products requiring high water consumption, are observed to increase significantly in planting areas.

As of the end of 2012, the number of groundwater wells in the basin exceeded 130,000. Of these, about 27,000 are

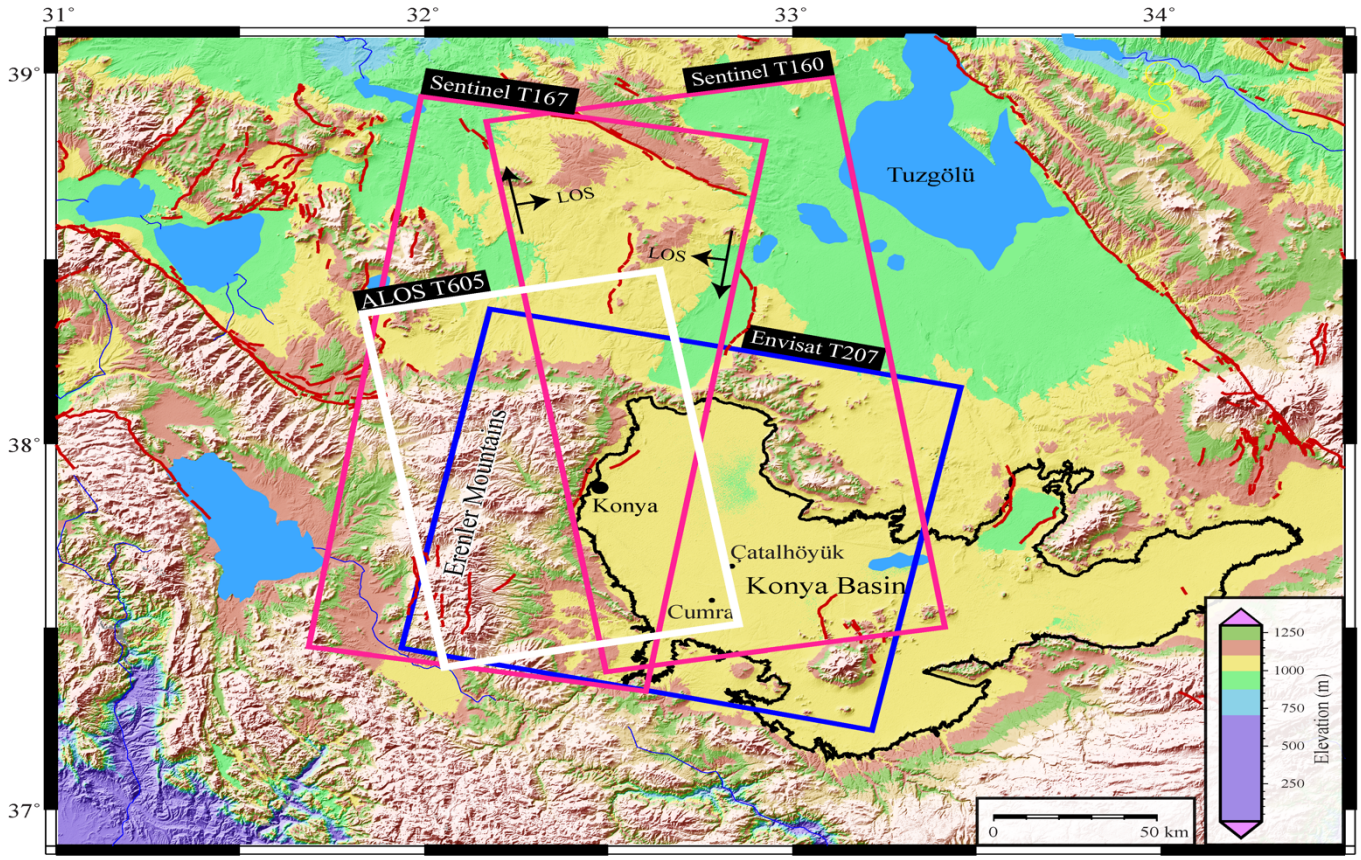

Figure 1. Morphotectonic map of the Konya basin and its vicinity with shaded relief image from the Shuttle Radar Topography Mission (SRTM) 90-m posting data. Red lines are active faults (from Emre et al., 2013). Rectangles show SAR image frames used in this study. While ALOS-1 T605 and Sentinel T160 are on ascending orbits, Envisat T207 and Sentinel T167 are on the descending orbits. Arrow couples show the satellite flight direction and radar line of sight (LOS). The black line represents the boundary of the Konya Plain that corresponds to ~1050 m elevation above sea level.

licensed only (WWF-Türkiye, 2014). As a result of excessive ground water extraction, sinkholes reaching to hundred meters in depth and diameter occur in Konya almost every year.

3. Geology of the study area

The ongoing tectonic regime in Konya and its surrounding regions is known as the "Ova regime" (Şengör, 1980) and "Central Anatolian neotectonics regime" where tectonic activity is insignificant, except some localized minor strike-slip and normal-slip related deformation (Kocyiğit et al., 2000).

Konya city lays on the flat Quaternary alluvium to the east of the Erenler mountains where basement rocks crop out (Figures 2 and 3). The basement rocks consist of various types of lithology with ages from Paleozoic to Cenozoic (Eocene). It is made up of Late Permian-Early Cretaceous meta-carbonates and meta-clastic representing shallow marine rocks in origin, and Late Cretaceous metamorphosed pelagic and olistostromal rocks (Hakyemez et al., 1992). These rocks are over thrusted by metamorphosed Late Cretaceous ophiolitic mélange and Mesozoic ophiolite (Şengör and Yılmaz, 1981). All these rocks are covered unconformably by the Paleocene-Eocene unmetamorphosed, shallow-marine clastic. Miocene-Quaternary continental rocks are the youngest unit of the region. The subduction of the Late Permian Cretaceous rocks, which are part of the passive continental margin of the Menderes-Taurid block, under the Kırşehir block developed obduction of ophiolite and HP/LT metamorphism (Şengör and Yılmaz, 1981). The final suturing in the region produced low-degree greenschist metamorphism and imbricated structures (Şengör and Yılmaz, 1981). Western part of the city sits on alluvial fans that formed in front of the Erenler mountains that have been deeply incised by streams (Figure 2). The thickness of the Quaternary alluvium and alluvial fans in this area is not known.

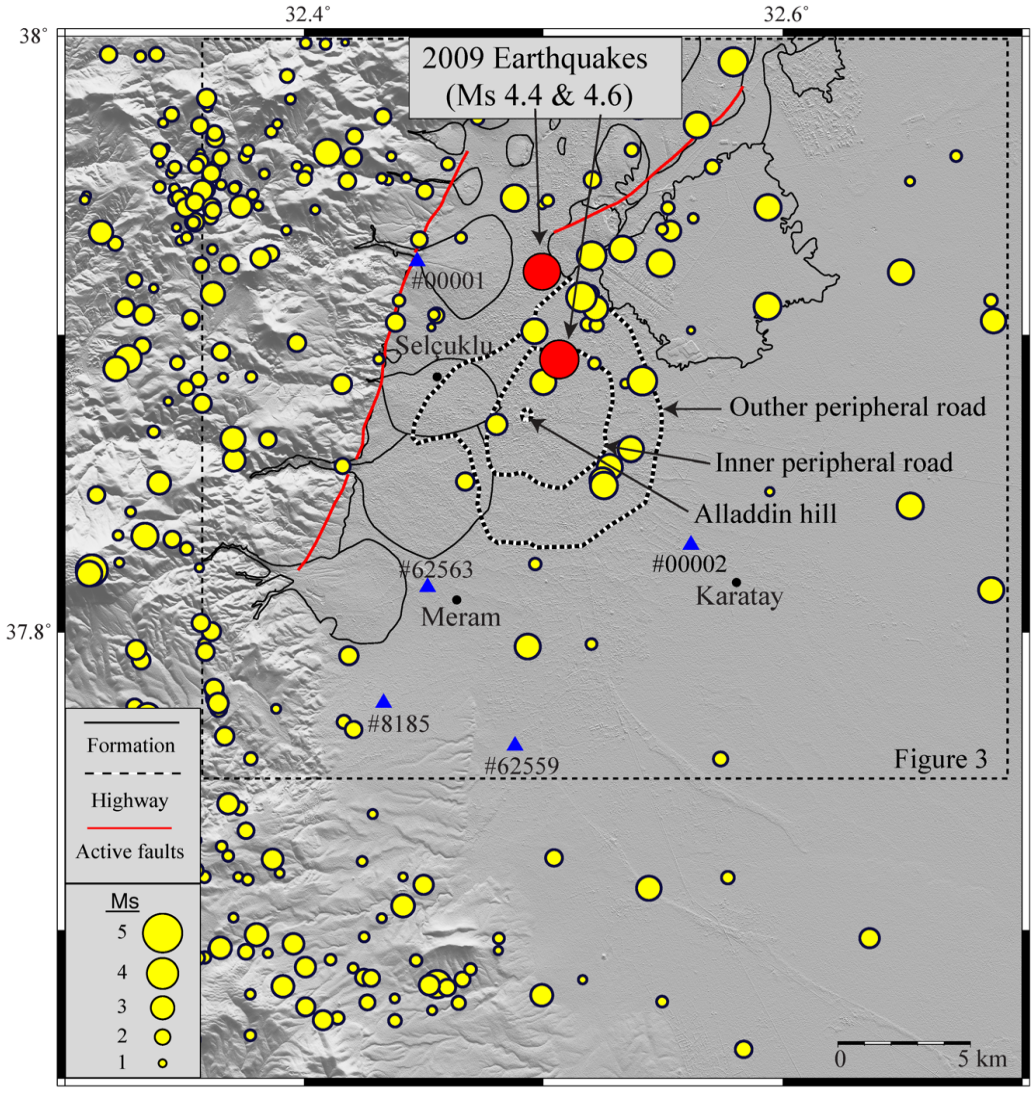

Figure 2. (a) Seismicity of the study area since 1990 from AFAD with active faults (red lines) and black polygons that show the boundaries of alluvial fans and other lithology in the alluvial plain. White dashed lines show peripheral roads with Alaaddin Hill in the center. Blue triangles with numbers indicate locations of wells from The General Directorate of State Hydraulic Works (DSI).

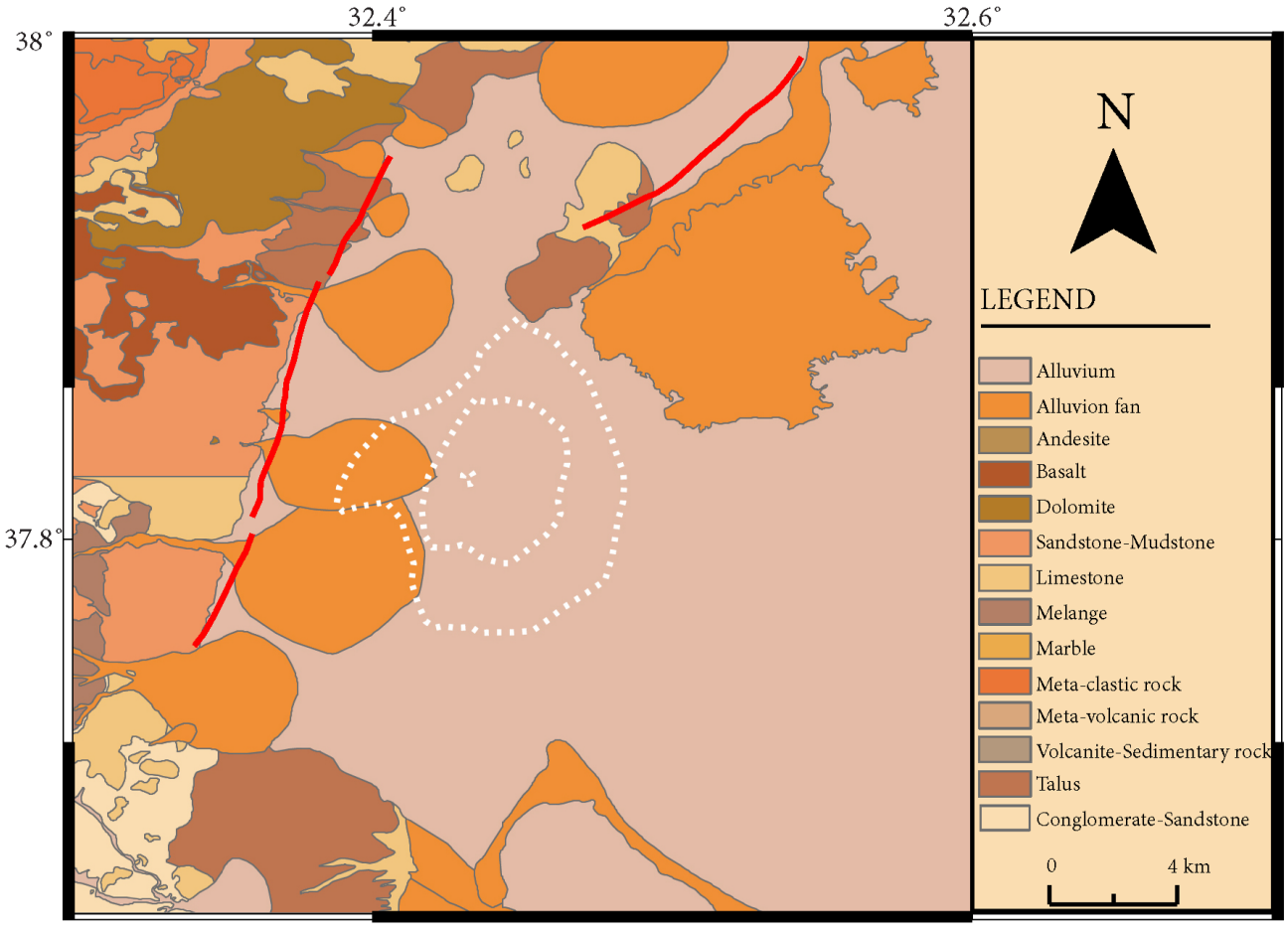

Figure 3. Geological map of Konya and its vicinity based on 1:25.000 scaled maps of MTA.

There are only two active fault segments mapped by MTA (General Directorate of Mineral Research and Exploration of Turkey) (Emre et al., 2013) in the study area (Figure 2). Located along the foothills Erenler Mountains about 6 km west of the city center, the main Konya fault separates the basement rocks from the Quaternary alluvium. The other fault is located about 5 km to the north in the alluvial plain. Both faults appear to be normal faults. Seismicity recorded by the Directorate of Disaster Affairs (AFAD) between 1990 and 2021 is relatively low in the study area, and earthquakes are scattered and have magnitude mostly below 4 (Figure 2). However, in 10–11 September 2009, the region was struck by two earthquakes with magnitude 4.4 and 4.6 and depths around 5 km (AFAD). Focal mechanisms from INGV (National Institute of Geophysics and Volcanology of Italy) indicates that the earthquakes took place on a normal fault dipping roughly eastward, consistent with the geometry of the Konya fault (Aksoy and Demiröz, 2011). Therefore, Aksoy and Demiröz (2011) suggest that the events took place on the Konya fault that dips towards east-southeast. No significant damage or any loss of lives during these earthquakes were officially reported. However, since the earthquake shaking was amplified by the poor dynamic characteristics of the soil, slight damages to some buildings occurred, which, according to Aksoy and Demiröz (2012), is due to the poor-quality construction of buildings built on alluvial soils.

4. SAR data and methodology

To investigate the evolution of the subsidence since the early 2000s, we used C-band (~5.5 cm wavelength) data obtained by Envisat ASAR and Sentinel-1 A/B images acquired from 2004 to 2010 and 2014 to 2020 respectively, and L-band SAR data (~24 cm wavelength) obtained by ALOS-1 PALSAR images acquired between 2006 and 2010 (Figure 4). Envisat and Sentinel data of the European Space Agency are freely available. Whereas, the ALOS-1 satellite data of the Japanese Aerospace Exploration Agency can be obtained through proposals for scientific research. While Sentinel images were acquired on both ascending (T160) and descending (T167) orbits, ALOS-1 and Envisat data are on ascending and descending tracks, respectively (Fig. 1). Thus, we have SAR images that were acquired on two ascending and two descending orbits on different time periods between 2004 and 2020. While in each Sentinel-1 A/B track the number of images since 2014 is over 250 (256 images on T160 and 258 images on T167), the number of images on ALOS-1 and Envisat is only 16 and 37, respectively (Figure 4). The abundance of the Sentinel data is owing to 12-day repeat cycle of the Sentinel satellites, which follow each other 6 days apart since the launch of Sentinel 1B in April 2016 about two years after Sentinel 1A. The study area is entirely covered by all SAR datasets used in this study.

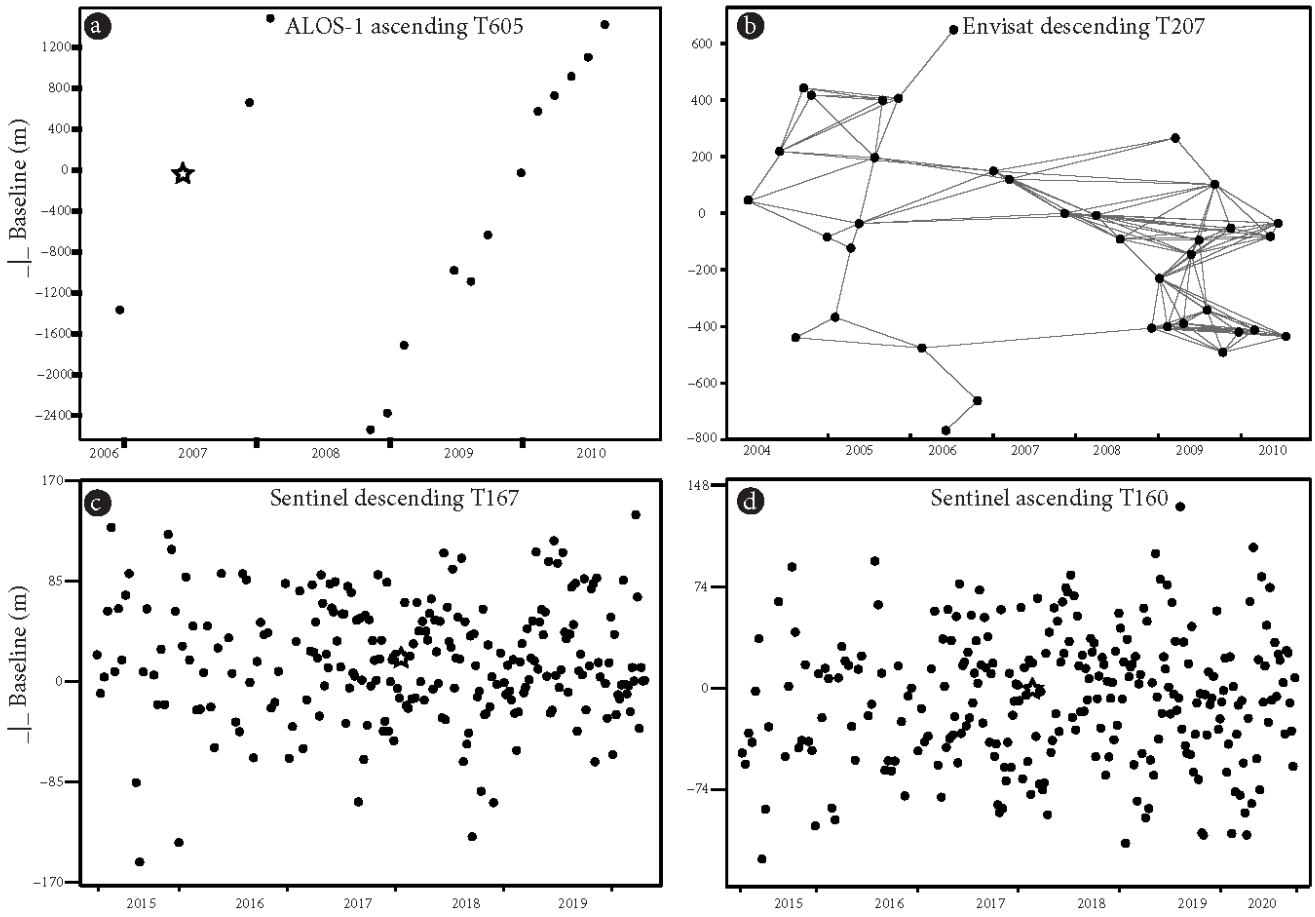

Figure 4. Plot of perpendicular baselines versus time of ALOS-1 (a), Envisat (b) and Sentinel-1 A/B (c, d) images used to calculate the deformation field in Konya (see Figure 1 for their location). Black dots indicate the SAR image and white stars indicate the reference image chosen for time series analyses. Grey lines indicate interferogram pairs for Small Baseline InSAR time series analysis for Envisat data with perpendicular and temporal baselines up to 250 m and of 2.5 years, respectively (d).

To map surface deformation in Konya city, we use the Synthetic Aperture Radar Interferometry (InSAR) technique, which combines two SAR images of a given area to form an interferogram (Gabriel et al., 1989; Massonet et al., 1993). The phase of each pixel in the interferogram is the difference between the phase of the corresponding pixels in each of the two images. The phase change results mainly from (1) changes in atmospheric conditions (mainly water vapor) during the acquisition of the two images, (2) errors in orbital parameters estimations, (3) topographic relief, and (4) motion on the Earth's surface. To isolate surface motions, orbital and topographic phases can be eliminated from an interferogram with a removal of a planar ramp and simulated phase based on precise digital elevation models, respectively. Atmospheric phases are, however, difficult to be separated due to their turbulent nature. If atmospheric phases result mainly from stratified troposphere, they can be visually detected, modeled and removed to some degree from interferograms as they are correlated with topographic elevation. In order to eliminate atmospheric noise and residuals due to errors in digital elevation models, advanced InSAR techniques such as Persistent Scatter InSAR (PS-InSAR) (Feretti et al., 2001; Hooper, 2008; Hooper et al., 2011) and Small Baseline Subset InSAR (SBAS) (Berardino et. Al., 2002) are used when multiple (> 12) SAR images are available in a region of interest. While ALOS and Sentinel time series are calculated using the PS-InSAR technique, the Envisat time series are obtained using SBAS. These multi temporal InSAR (MT-InSAR) techniques allow for millimeter precision ground deformation mapping by computing displacement time series of each stable Permanent Scatterer pixel in an area.

To calculate interferograms from Envisat, ALOS and Sentinel-1 A/B images covering the Konya city, we use freely available open-source software tools; while all Sentinel interferograms are calculated using GMTSAR (Sandwell et al., 2011), ALOS-1 and Envisat raw images are focused (to single look complex images) by ROI_PACK (Rosen et al., 2000) and then processed with DORIS (Kampes et al., 1999) to form interferograms. 1-second posting (~30 m) SRTM digital elevation data are used to remove the topographic phase from the interferograms. All the processing has been carried out at TUBITAK ULAKBIM, High Performance and Grid Computing Center (TRUBA resources). To generate maps of surface deformation over Konya city, we use the Stanford

Method for Persistent Scatterers (StaMPS) package (Hooper, 2008; Hooper et al., 2011) that takes advantage of the spatial correlation between pixels. StaMPS uses only the selected pixels that show stable phase noise characteristic in time to compute average velocities and time series. This method is considered to be a modified version of PS algorithm and applicable in areas undergoing non-steady deformation, such as aseismic slip, without using prior knowledge of the temporal deformation model. Time series in all different data tracks, except the Envisat, are obtained with a single reference network for PS-InSAR analysis. The reference images are chosen from summer time periods and optimal spatial and temporal baselines (Figure 4). Envisat data are analyzed with the SBAS algorithm incorporated in StaMPS.

5. Surface deformation since 2004

Mean line-of-sight (LOS) velocity maps calculated from InSAR time series using Envisat, ALOS-1 and Sentinel images are shown in Figure 5. LOS velocities are obtained mostly over the settlements, engineering structures and non-vegetated mountainous regions in the west of the city where coherence is relatively high for PS-InSAR and SBAS analysis. Areas with blue colors indicate stable regions and those that move toward to satellite (i.e. uplift or horizontal motion opposite of the satellites' look direction), whereas colors from yellow to red show regions away from satellite (i.e. subsidence or horizontal motion in the satellites' look direction). Grey regions are places where no permanent scatterers or coherent phase for SBAS inversion were found in the time series processing. While ALOS-1 velocity field is available almost everywhere over the entire image frame due to its higher signal wavelength (~24 cm), Sentinel data do not provide useful data over the cultivated regions of the Konya basin due to loss of coherence resulting from long temporal baselines (~3 years) and lower signal wavelength. Similar to the ALOS-1 velocity field, useful data in the Envisat images are also abundant not only in the city but also in the agricultural regions to the west. Note that subsidence is taking place in flat parts of the city with no motion in the hills to the west where the Konya fault is located (Figure 6).

All the velocity fields of different periods show a similar pattern of deformation in the Konya Metropolitan area,

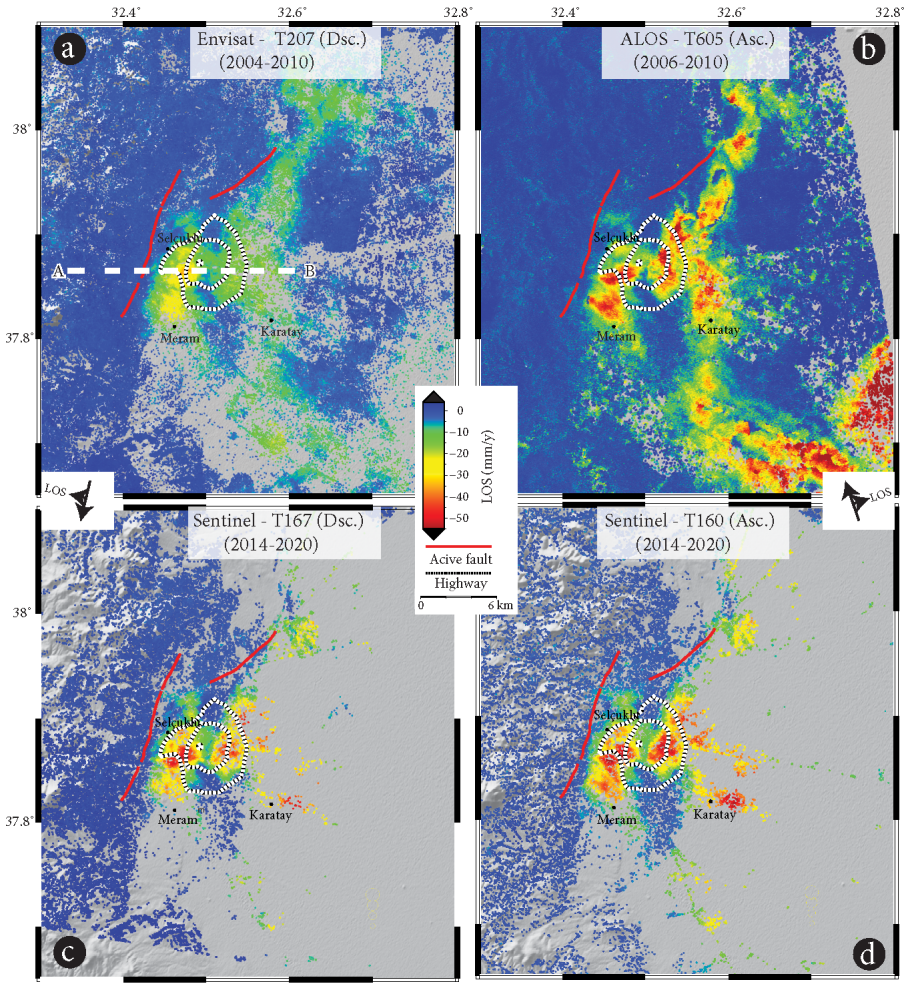

Figure 5. InSAR LOS velocity fields calculated from InSAR time series using ENVISAT (a), ALOS-1 (b) and Sentinel-1 (c, d) images. Warm colours (green to red) show displacement away from the satellite (subsidence or horizontal motion in LOS look direction), cold colours (blue) indicate stable areas and displacement toward (uplift or horizontal motion in the opposite LOS direction) the satellite. White dash line shows the location of the profile shown in Figure 8.

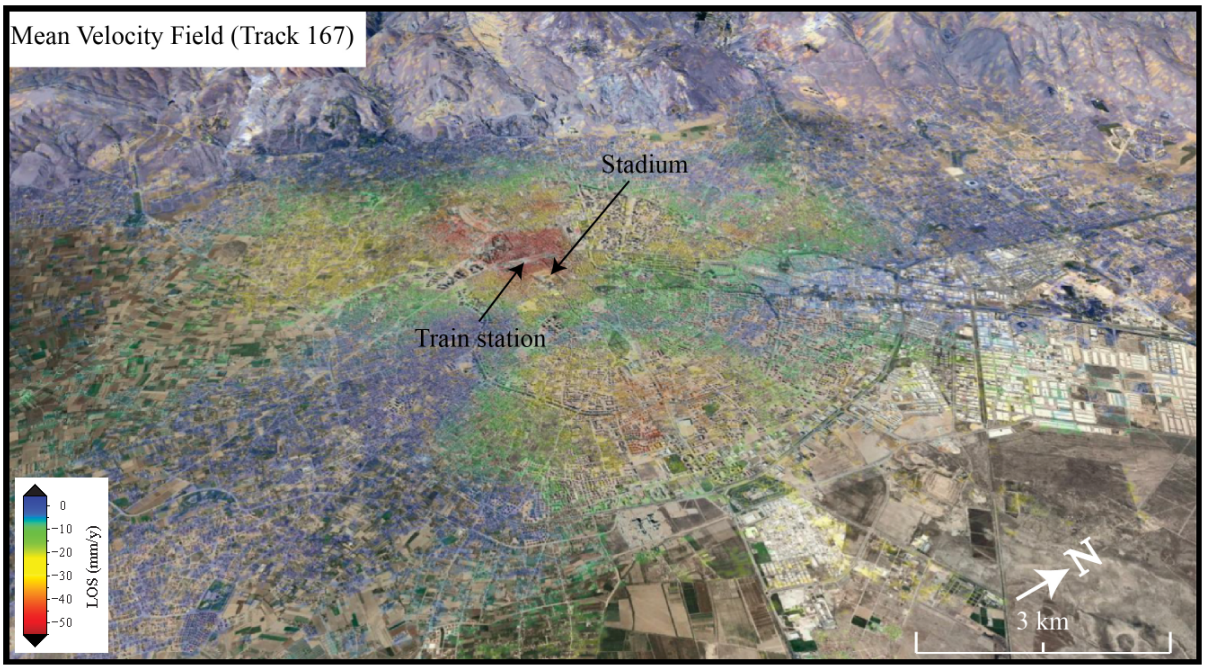

Figure 6. Mean velocity field in line-of-sight direction obtained from Sentinel descending track T167 superimposed on 3-Dimensional Google Earth image (view towards west).

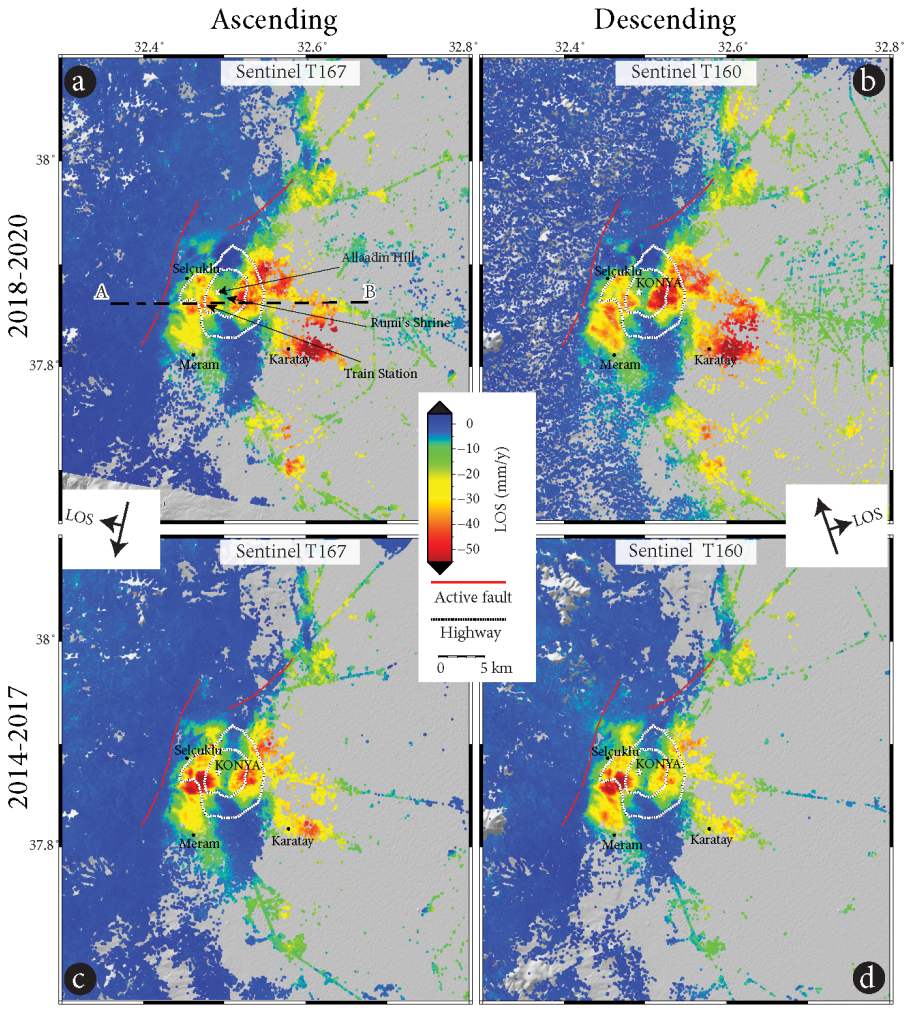

Figure 7. InSAR LOS velocity fields calculated from Sentinel data at two different periods 2018–2020 (a, b) and 2014–2018 (c, d). Note that while subsidence rate increases on eastern side of the city since 2018, it decreases in the western side.

implying that LOS changes seen in the maps are mostly due to vertical deformation with negligible horizontal and atmospheric effects. The differences are due to different viewing geometry and differences in the observation periods. Although less pronounced in the Envisat velocity field, there are two lobes of subsidence reaching locally 7 cm/yr in LOS direction in the western and eastern sides of the city, in good agreement with Orhan (2021) who used the Sentinel-1 data on track T167. These two regions are separated by an approximately N-S zone that divides the city nearly into equal halves.

It is clear from the Envisat results that subsidence was much slower initially and increased with time. In order to reveal the spatiotemporal evolution of the subsidence, we have also processed the Sentinel data at different time windows: 2014–2018 2018–2020. Analysis of mean velocity fields obtained from different time windows shown in Figure 7 reveals that subsidence varies in time and space over the last 6 years as well.

To better visualize the variation of subsidence over time and space, profiles are taken from the mean LOS velocity fields in east-west direction crossing the center of maximum subsidence in both lobes (Figure 8). LOS velocities are converted to vertical velocities assuming that deformation is purely vertical so that one can compare subsidence rate measured by different look angles. This is because sensitivity of satellites to vertical or horizontal motions varies with varying look angles. Profiles in Figure 8a show very clearly that subsidence increased in both lobes from a few cm/yr up to 9 cm/yr between 2004 and 2018. However, between 2018 and 2019, while subsidence in the western lobes remains nearly the same, subsidence in the eastern lobe increases from 6–7 cm/yr to 11 cm/yr (Figure 8b). After 2019, both lobes start shrinking very rapidly, especially the western lobe (Figure 8c). However, subsidence in the eastern lobe is still taking place at a significant rate (7 cm/yr).

Temporal evolution of subsidence at selected locations of the city can also be seen in Figure 9. Time series in LOS direction show that while subsidence rate fluctuates with time due to the seasonal effects in the agricultural fields to the east (e.g., time series #2), it is highly linear in the metropolitan areas. This suggests that, unlike in the agricultural regions, in most metropolitan places, the ground water is continuously extracted nearly at a constant rate, which in turn implies that water extraction is carried out most probably to supply drinking water to the rapidly expanding Konya city (Orhan, 2021). Time series #2 shows dramatic drop in groundwater despite the pauses in winter, during which little or no recovery is achieved. Subsidence at site #1 north of the city has been recovering since mid 2018.

Variation of subsidence in space and time in the Konya metropolitan area implies that subsidence is also caused by over extraction of groundwater, just like in the agricultural fields to the east (Orhan, 2021). Indeed, visual inspection of interferograms reveals the presence of numerous concentric fringes, each probably centering around a groundwater pump scattered around the city (Figure 10). Individual concentric fringes merge with each other with time and form the large lobes we observed in the mean velocity fields.

6. Decomposition of InSAR LOS velocity maps

Only the Sentinel satellites capture the subsidence in the study area from both ascending and descending orbits. Therefore, we can retrieve two of the three components of the actual deformation vector into horizontal (east-west) and vertical direction by decomposing the mean LOS velocity fields on the ascending and descending tracks. In a first step, the mean 2014-2018 line-of-sight velocities for the ascending and descending Sentinel tracks are resampled onto a 100 × 100 m regular grid, which is used as input for displacement decomposition. A nearest neighbor procedure is used to resample the persistent scattered pixels that are within 200 m of the center of each grid nodal point. In a second step, all the pixels that exist in both the ascending and descending tracks are selected. Before decomposition, InSAR mean velocity fields of both tracks referenced into the same reference frame using a reference area considered as a stable area (blue regions are assumed zero). In the last step, the line-of-sight velocity fields are decomposed into two components: the horizontal component along east-west direction (d_{hor}) and the vertical component (d_{ver}) were computed, taking into account the local incidence angle of the satellite view by solving the following equation (Motagh et al., 2017).

$$\begin{pmatrix} d_{asc} \\ d_{dsc} \end{pmatrix} = \begin{pmatrix} \cos\theta_{asc} & -\cos\alpha_{asc}\sin\theta_{asc} \\ \cos\theta_{dsc} & -\cos\alpha_{dsc}\sin\theta_{dsc} \end{pmatrix} \begin{pmatrix} d_{ver} \\ d_{hor} \end{pmatrix} \quad (1)$$

where θ_{asc} and θ_{dsc} represent the local incidence angles and α_{asc} and α_{dsc} are the satellite heading angles in ascending and descending modes, respectively.

Figure 11 shows vertical and E-W velocity fields obtained after the decomposition. Decomposition results confirm that most of the LOS deformation is in the vertical direction, that is subsidence. Horizontal motions are in general results from vertical motions and, as expected, while westward motions are located in the eastern sides of LOS lobes, eastward motions are located in the western sides. Profiles of vertical and horizontal velocities along the line A-B illustrate the relationship between the horizontal and vertical motions as eastward motions (positive values) are located at the western edges of the lobes and westward motions (negative values) at the eastern edges of the lobes (Figure 12). It is worthwhile to note that infrastructure and building damage as a result of subsidence should be expected in areas where gradients of vertical and horizontal deformation are steep.

7. Relationship between InSAR time series and groundwater wells

To investigate the relationship between subsidence and hydro-geological activities on the area, we have obtained piezometric measurements from DSI (State Hydraulic Works of Turkey). Unfortunately, none of the DSI wells are located in the metropolitan area of the city where significant subsidence is taking place (Figure 13a). Nevertheless, even though these piezometric measurements near the basement not indicate rapid changes in ground water table with time, they are still correlated with the PS-InSAR time series taken

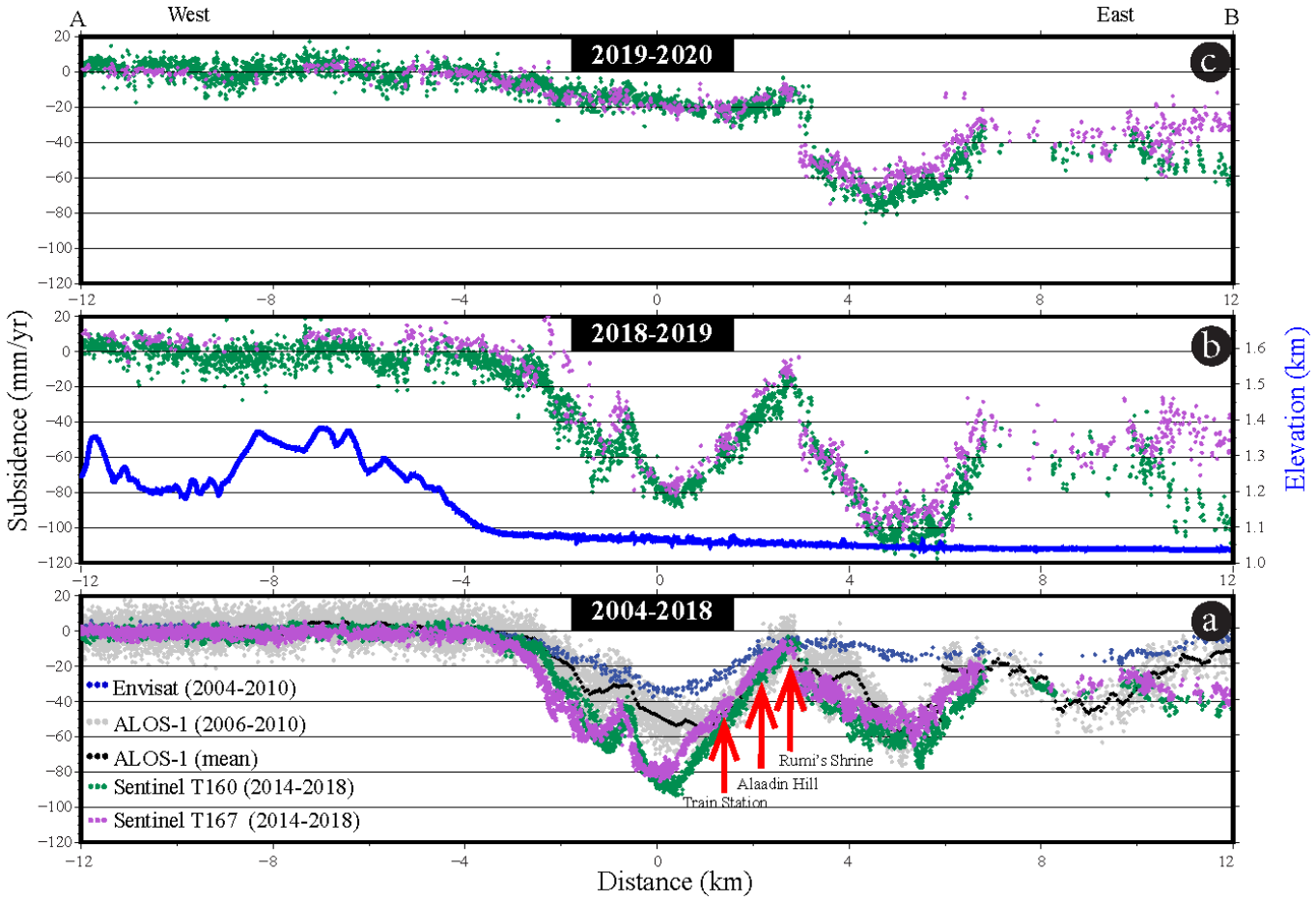

Figure 8. Vertical velocity profiles along line A-B shown in Figure 5. The shift in the center of subsidence in Sentinel data, which is due to difference in viewing geometry in ascending and descending orbits. Note the overall increase in subsidence rates between 2004 and 2018, and rapid decrease after 2019.

from Sentinel dataset of tracks T160 and T167 (Figure 13b). On the other hand, the InSAR time series and the groundwater table levels in wells on the alluvium are highly correlated, confirming that subsidence in the region results from excessive ground water extraction as reported by Caló, et al. (2017) and Orhan (2021) (Figure 13b). In some wells, drop of the groundwater table reaches 15 m between 2014 and 2018. Analysis of the time series in Figure 13b shows that ~1.4 cm of subsidence occurs for every 1 m drop of ground table. Thus 8 cm/yr subsidence suggests 6 m drop of water table every year.

8. Elastic dislocation modeling

It is clear that the subsidence in the metropolitan area of Konya is also due to excessive ground water extraction as in the agricultural fields to the west. However, in order to investigate if part of the subsidence in the metropolitan area can be due to aseismic slip on the Konya fault below the city, we model the subsidence signal between 2014 and 2018 with elastic dislocations on a rectangular fault buried in a homogenous and elastic medium (Okada, 1985). Therefore, a model fault of 6 km long is placed along the surface trace of the Konya fault with an eastward dip of 45° (Figure 14).

Taking a forward approach, that is by a trial and error, a first order fit to contour lines of the observed deformation was obtained with 90 cm of pure normal slip at depths between 4 and 5 km. As shown in Figures 14 and 15, the model explains the overall subsidence pattern in the western side of the city but fails to mimic the eastern lobe as it requires highly heterogeneous slip and/or complex curvature down dip in the fault plane. Various models with similar fit were also obtained by playing with the depth, dip and amplitude of slip. However, models with slip less than 70 cm, dip less than 45°, and depth shallower than 3.5 km cannot explain the overall pattern of subsidence. All the models require a moment magnitude, Mw > 5. Therefore, subsidence in the metropolitan areas of Konya cannot be explained with fault activity at depth because such a high amount of aseismic slip is not plausible.

If the subsidence is due to compaction of alluvial sediments that, in turn, results from to dropdown of the groundwater table, it can be modeled by negative opening (i.e. volume loss or compaction) on a surface enveloping the water table. For modeling the observed land subsidence above, we use Poly3Dinv inversion software (Maerten et al., 2005) that uses Poly3D, a 3D-boundary element method with triangular dislocations in a linear-elastic and homogeneous half-space and a damped least-square minimization (Thomas, 1993). A

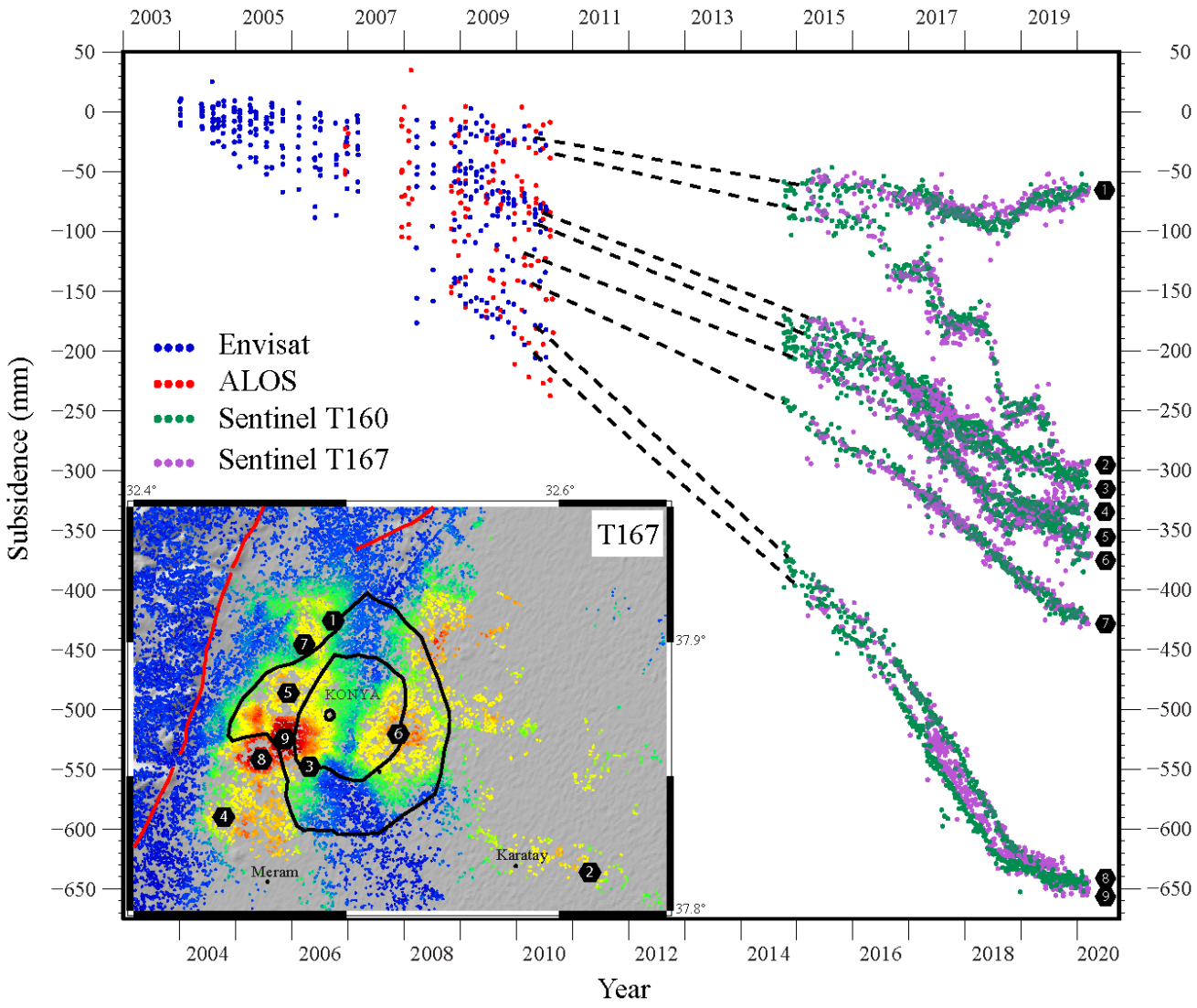

Figure 9. Evolution of subsidence with time. Time series at 9 different locations showing the subsidence in the metropolitan areas of Konya city since 2004. Sentinel time series are aligned with Envisat and ALOS-1 time series assuming that the sites were undergoing subsidence with a constant rate between 2010 and 2014. Note the slowdown of subsidence on the western side of the city since 2019 (#8 and #9).

surface with triangular elements is constructed at a depth of 150 m, which appears to be roughly the depth of groundwater table in this region. The size of triangles becomes smaller towards the center of the western and eastern lobe of subsidence so that the gradient of subsidence can be mimicked with opening (Figure 16). Modeling results show that subsidence between 2014 and 2018 in Konya and its vicinity gives rise to a volume loss of 770 m^3 every year due to compaction of sediments. This is just for the region included in the model. The volume loss in the entire basin is naturally far more than this and reaches probably millions of cubic meters. If the ground water table is lower than 150 m, the volume loss will be higher. Answering to how much of this compaction is recoverable requires monitoring and measuring amount of uplift following the cease of groundwater extraction in an area. Such an area is observed north of the city where time series (#1 in Figure 9) indicate about 3 cm of uplift since mid 2018.

9. Discussion and conclusion

MT-InSAR analysis of SAR images acquired by 3 different space borne sensors spanning different time periods shows that the city of Konya has been subsiding since 2004. Subsidence is confined to the Quaternary alluvium, while there is almost no deformation in the hills to the west of the city where the active Konya fault is located. The pattern of subsidence shows two main lobes of rapid subsidence to the west and east of the city center with a N-S line of no deformation that divides the city into two nearly equal halves. The western and eastern lobes are centered in 500 m west of the train station and 5 km east of the train station, respectively. What separates the subsidence of the city two halves along a roughly north-south line is unknown. It may be due to lithological differences in the alluvium on which the city is built or presence of a fault that may be sealed and, hence, act as barrier to the aquifer system or the rate of extractions on both sides are not sufficiently high for lobes to

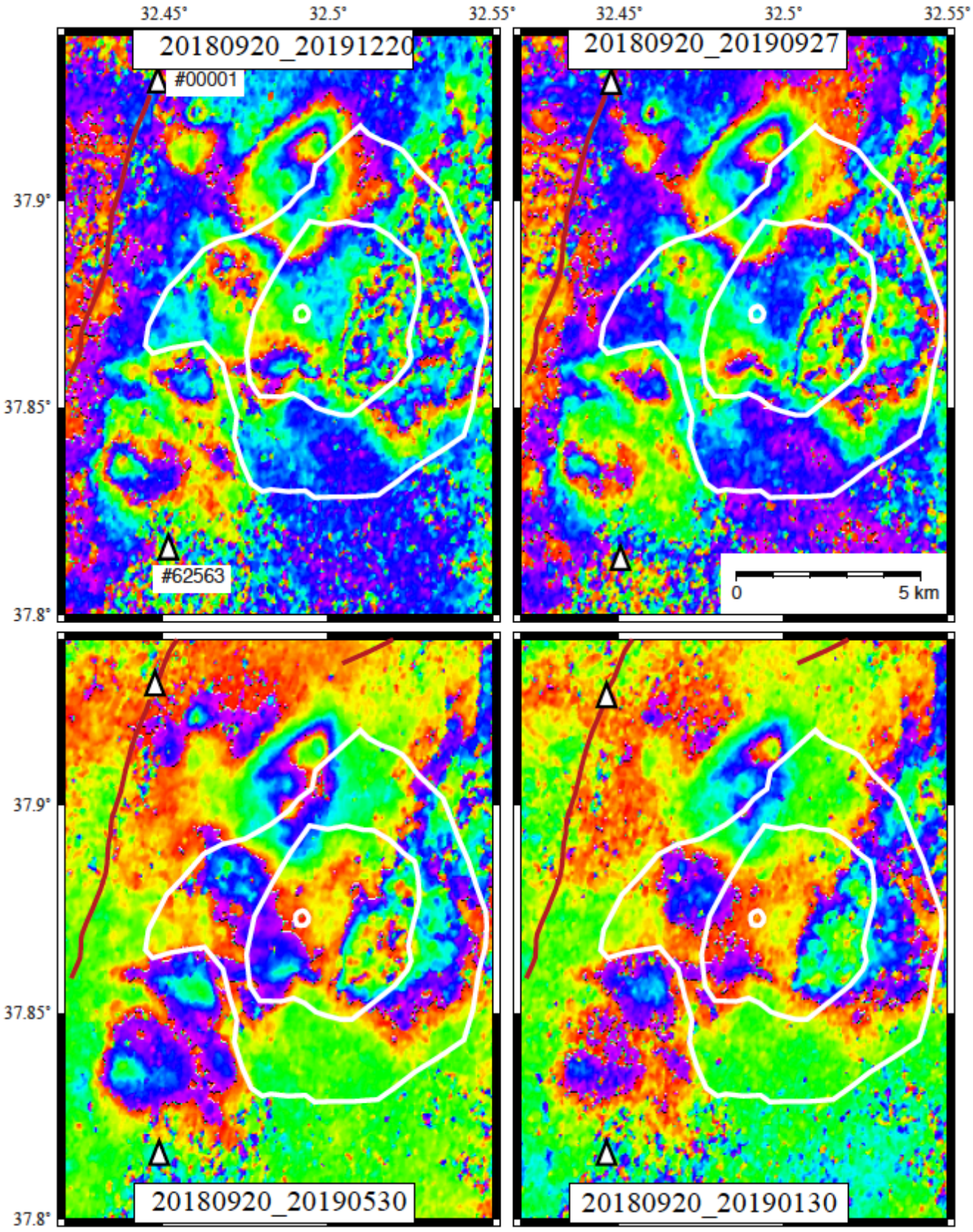

Figure 10. Selected interferograms from track T160 that display circular pattern of fringes centered most likely at wells from which ground waters are extracted. Triangles show locations of wells from DSI. White lines show peripheral roads at Konya city.

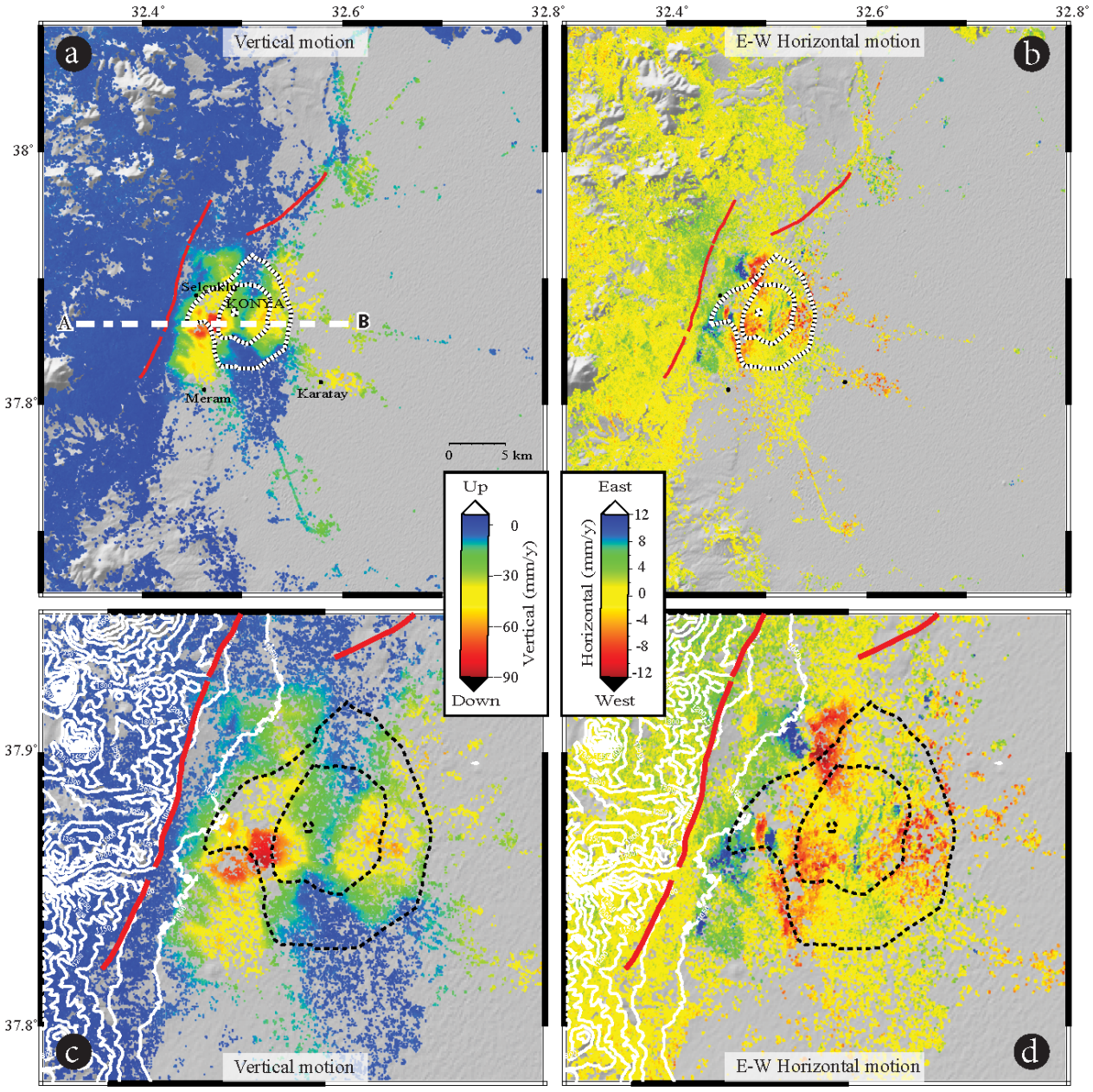

Figure 11. Vertical (a) and horizontal (b) components of the surface deformation calculated by decomposing LOS velocity fields on Sentinel ascending (T160) and descending (T167) tracks between 2014 and 2018. Close up view of vertical and horizontal velocity fields are shown in (c) and (d).

merge. Rate of subsidence increased from a few cm per year to 11 cm/yr between 2004 and 2019. Although subsidence has slowed down over the last two years, particularly in the western side of the city, it is still taking place at rates reaching 6–7 cm/yr in the eastern side of the city.

Spatiotemporal variation of subsidence and its strong correlation with change in water table level confirm that subsidence in the metropolitan area of Konya is due to overdrafting of the ground water used for urban needs. Over the last two years or so, the demand appears to have decreased as subsidence rate has slowed down dramatically or stopped at some places in the city. This appears to be due to the so called "blue channel" that transfers drinking water to the city from several recently built dams to the south.

In order to check whether or not subsidence can be partly explained by creep on down dip section of the Konya fault beneath the city, we have modeled the subsidence with elastic dislocations on a rectangular fault that coincides with the Konya fault. Modeling results show that an unrealistic rate of creep (about 10 cm/yr) is required on a small portion of the fault (about 6 km) at depths between 4 and 5 km. Thus, it is highly unlikely that part of the subsidence can be attributed to an aseismic slip on the Konya fault. We have modeled the subsidence with triangular dislocation in order to calculate

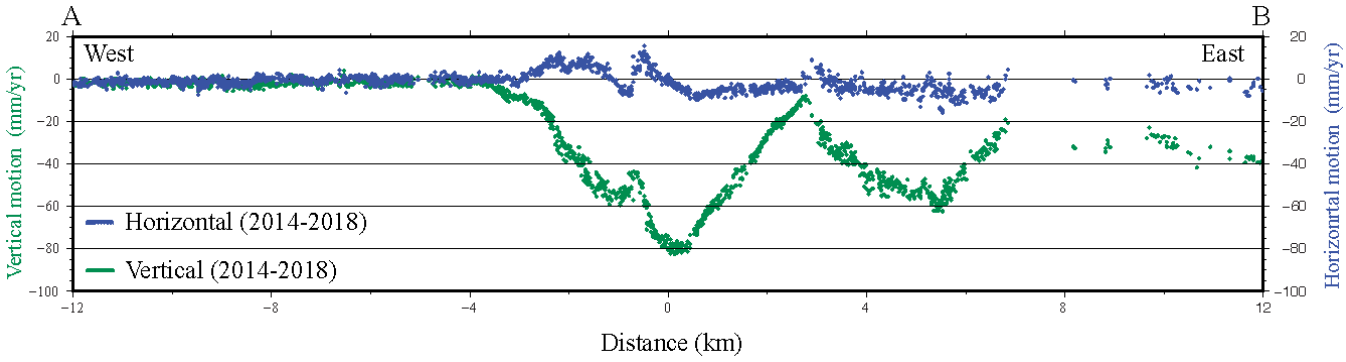

Figure 12. Vertical (green dots) and E-W (blue dots) velocity profiles along lines A-B shown in Figure 11. Negative positive horizontal values show westward and eastward motions, respectively. Note the increase in the subsidence rate from LOS to vertical component due to SAR viewing geometry and, hence, its sensitivity to horizontal and vertical motions.

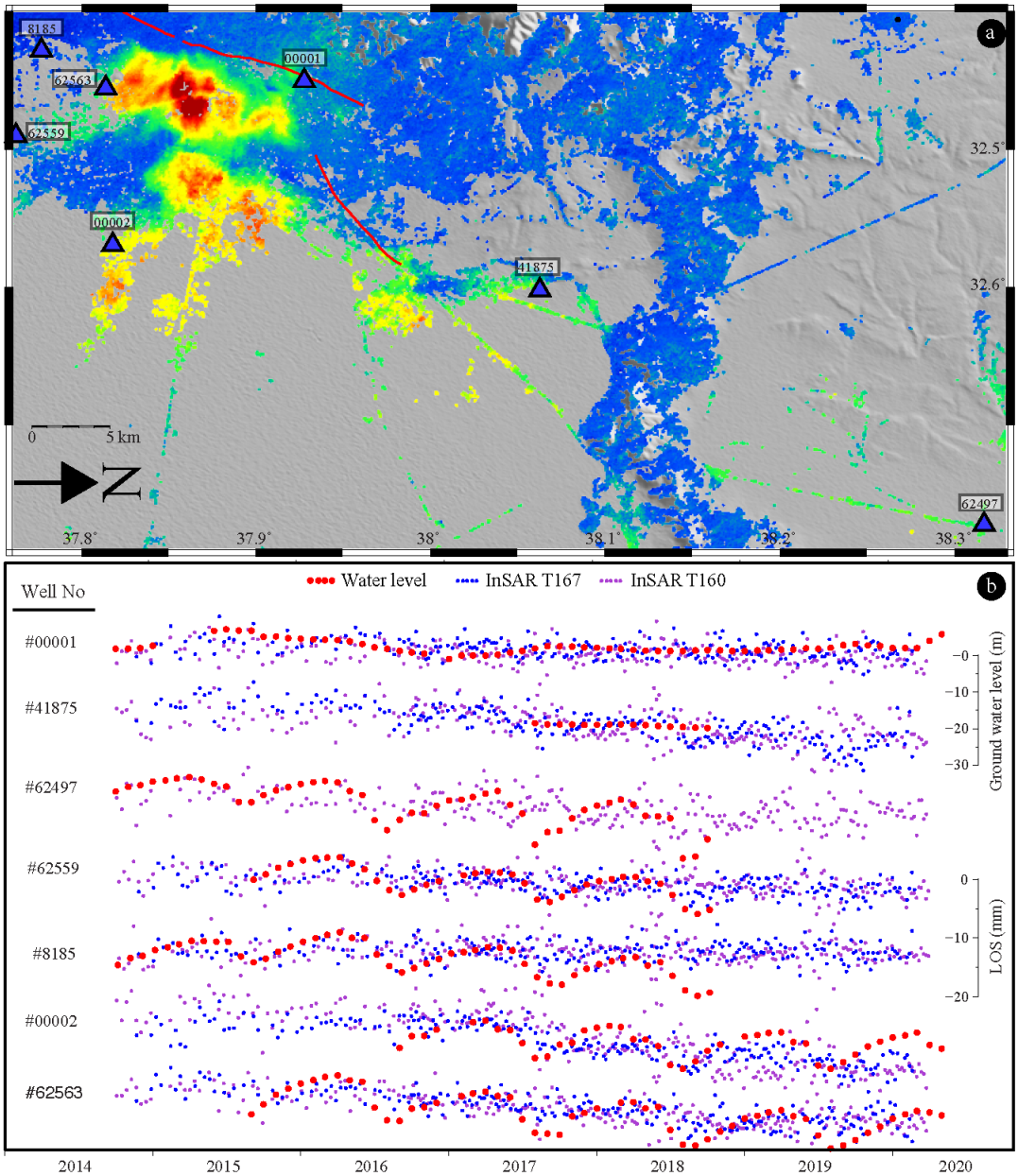

Figure 13. Correlation between subsidence and groundwater level change. **(a)** Location of available wells in the study area shown on the n LOS velocity field on T160. **(b)** Time series of InSAR together with piezometric measurements in the wells shown in (a).

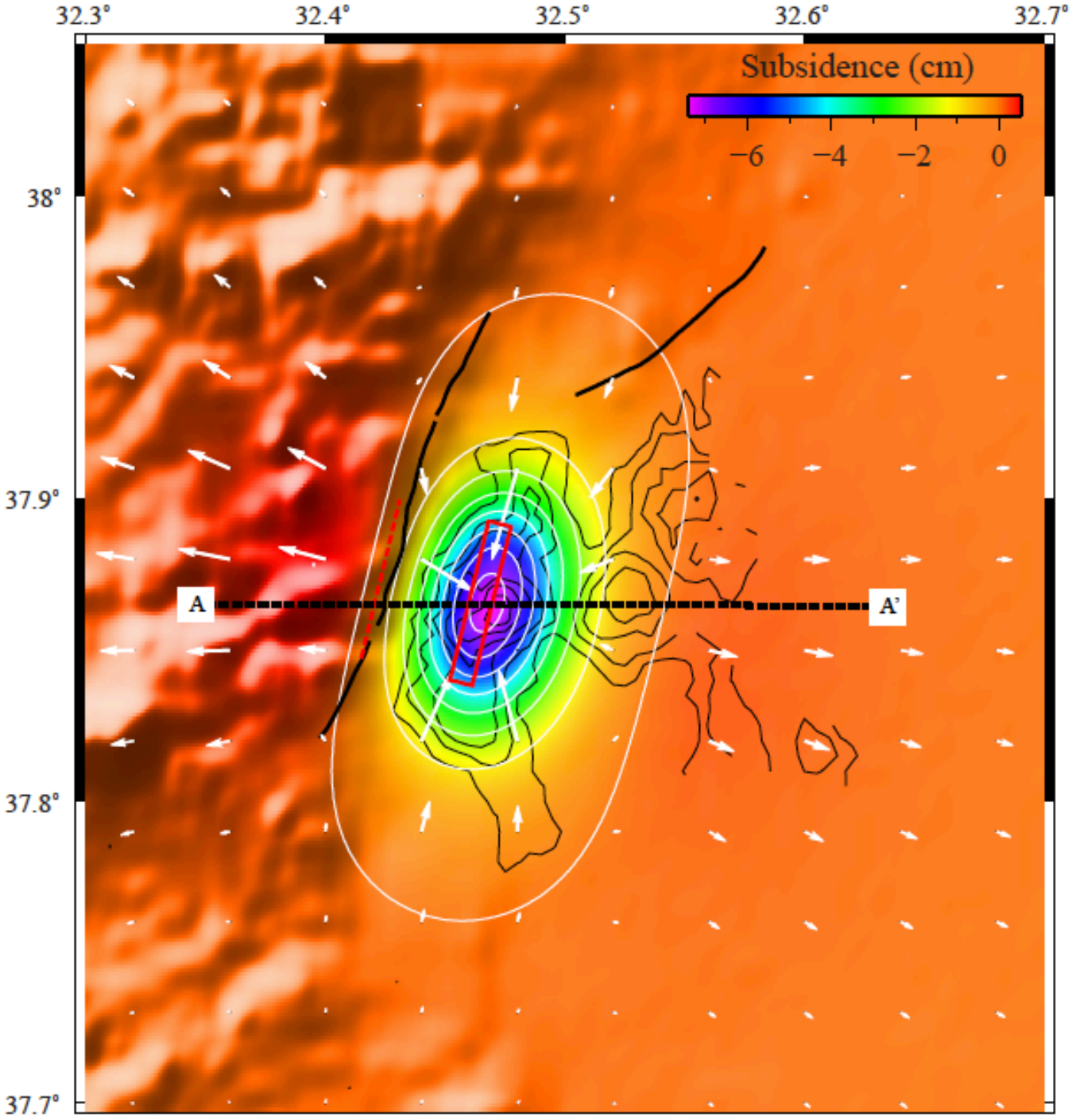

Figure 14. Elastic dislocation modeling results on the Konya fault. White and black contours are modeled and observed vertical deformation between 2014 and 2018 at 1 cm/y interval, respectively. While color coding indicates vertical motion, arrows indicate horizontal motion. Modeled fault at depth is shown with a red box whose surface projection (red dashed lines) coincides with the Konya fault. Black lines are active faults. Profile A-A' is shown in Figure 15.

volume loss due to compaction. The results show that every year a volume loss of ~7.7 x 10^6 m^3 is happening due to groundwater extraction. If the ground water extraction is totally stopped in the future, InSAR monitoring will answer the question of how much of this compaction is recoverable.

Although there is no reported incidence, subsidence taking place for decades must have caused significant damage to buildings and infrastructure in Konya, which needs to be investigated. The damage is probably visible in the form of fractures and tilts in engineering structures that we assumed are attributed to the low quality of buildings and materials.

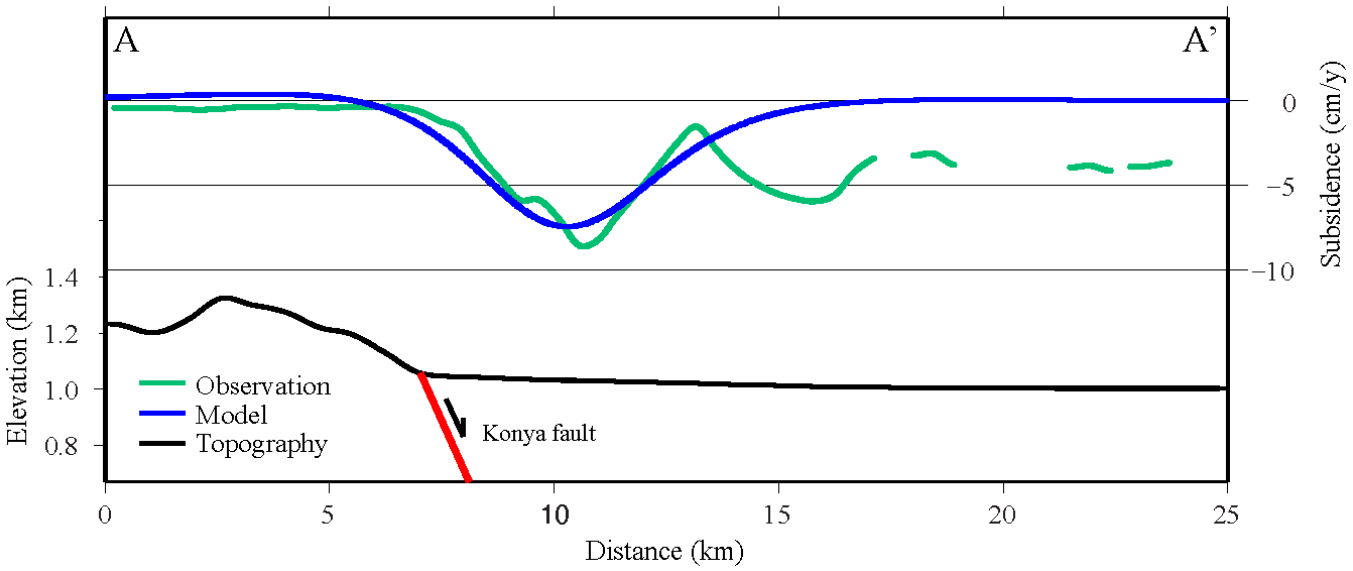

Figure 15. Profiles showing modeled (blue) and observed (green) subsidence due to potential slow slip on the Konya fault.

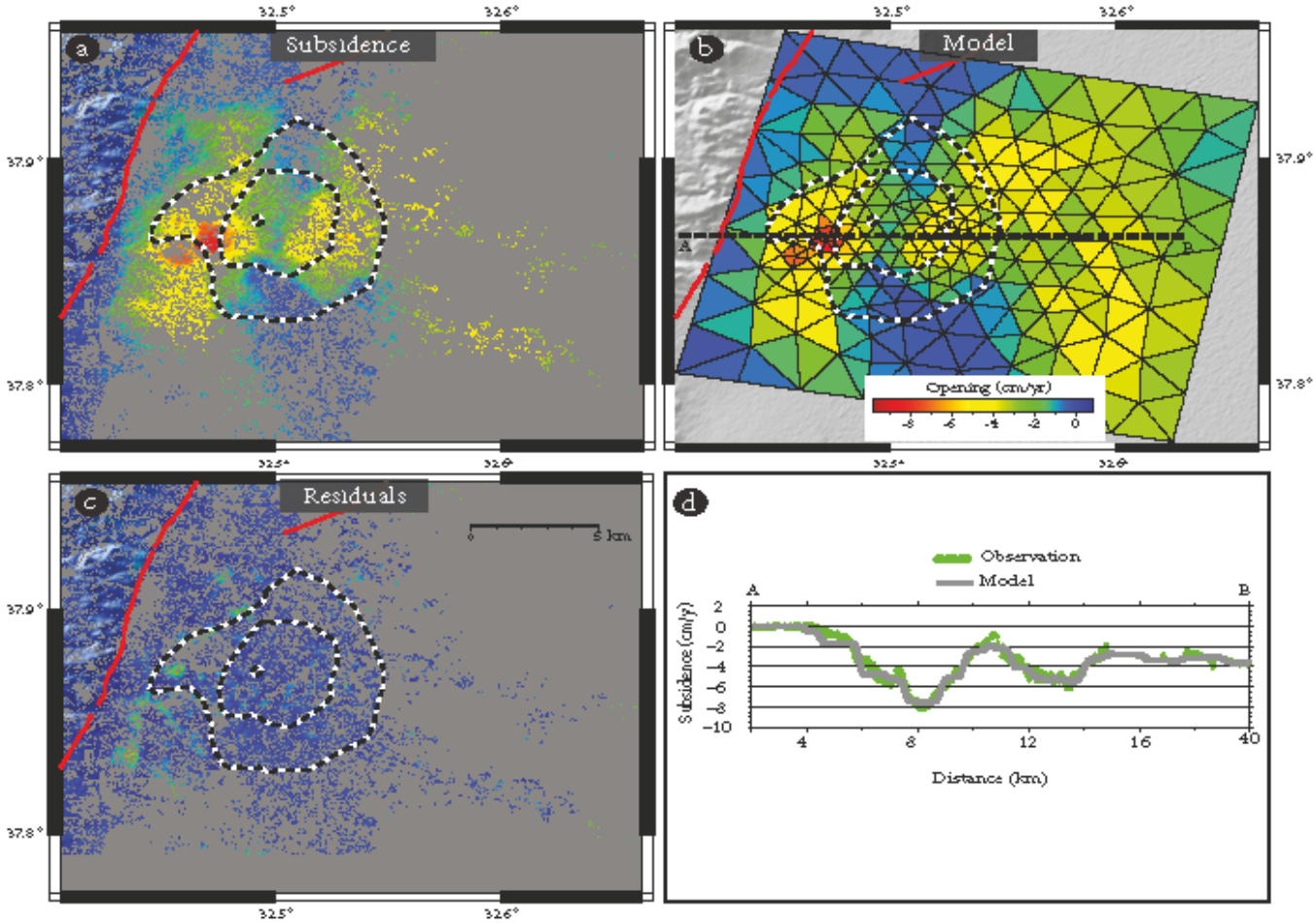

Figure 16. Modeling subsidence with the Poly3D boundary element method. Subsidence is modeled with negative opening (i.e. volume loss) on near horizontal plane that represents groundwater table at a depth of around 150 m. (a) Observed vertical deformation between 2014 and 2018. (b) Amount of opening on triangular elements at depths of about 50 m. (c) Residuals between observations and model predicted by opening. (d) Profile of observations and model along the line A-B.

Acknowledgments
This research was funded by İTÜ BAP Office through a project numbered MYL-2021-43033. InSAR processing was performed at TÜBİTAK ULAKBIM, High Performance and Grid Computing Center (TRUBA resources). We thank Prof. M. Sinan Özeren and Dr. Ahmet M. Akoğlu for sharing their ideas on modeling the subsidence in Konya.

References

Aksoy R, Demiröz A (2012). The Konya earthquakes of 10–11 September 2009 and soil conditions in Konya, Central Anatolia, Turkey. Natural Hazards and Earth System Sciences 12 (2): 295–303. doi: 10.5194/nhess-12-295-2012

Amelung F, Galloway DL, Bell JW, Zebker HA, Laczniak RJ (1999). Sensing the ups and downs of Las Vegas: InSAR reveals structural control of land subsidence and aquifer-system deformation. Geology 27(6): 483-486. doi: 10.1130/0091-7613(1999)027

Aslan G, Cakir Z, Ergintav S, Lasserre C, Renard F (2018). Analysis of secular ground motions in Istanbul from a long-term InSAR time-series (1992–2017). Remote Sensing 10 (3): 408. doi: 10.3390/rs10030408

Aslan G, Cakir Z, Lasserre, C, Renard F (2019). Investigating subsidence in the Bursa Plain, Turkey, using ascending and descending Sentinel-1 satellite data. Remote Sensing 11 (1): 85. doi: 10.3390/rs11010085

Bekaert DPS, Hamlington BD, Buzzanga B, Jones CE (2017). Spaceborne synthetic aperture radar survey of subsidence in Hampton Roads, Virginia (USA). Scientific reports 7 (1): 1-9. doi: 10.1038/s41598-017-15309-5

Berardino P, Fornaro G, Lanari R, Sansosti E (2002). A new algorithm for surface deformation monitoring based on small baseline differential SAR interferograms. IEEE Transactions on Geoscience and Remote Sensing 40 (11): 2375–2383. doi: 10.1109/TGRS.2002.803792

Berke MÖ, Dıvrak BB, Sarısoy HD (2014). Konya'da suyun bugünü raporu. WWF-Türkiye (Doğal Hayatı Koruma Vakfı) (in Turkish)

Caló F, Notti D, Galve JP, Abdikan S, Görüm T et al. (2017). Dinsar-Based detection of land subsidence and correlation with groundwater depletion in Konya Plain, Turkey. Remote sensing 9(1): 83. doi: 10.3390/rs9010083

Castellazzi P, Garfias J, Martel R, Brouard C, Rivera A (2017). InSAR to support sustainable urbanization over compacting aquifers: The case of Toluca Valley, Mexico. International journal of applied earth observation and geoinformation 63: 33-44. doi: 10.1016/j.jag.2017.06.011

Comut FC, Ustun A, Lazecky M, Perissin D (2016). Capability of detecting rapid subsidence with Cosmo SkyMed and Sentinel-1 dataset over Konya city. In: The ESA Living Planet Symposium ESA SP740; Prague, Czech Republic. pp. 9-13.

Du Z, Ge L, Ng AHM, Zhu Q, Yang X et al. (2018). Correlating the subsidence pattern and land use in Bandung, Indonesia with both Sentinel-1/2 and ALOS-2 satellite images. International Journal of Applied Earth Observation and Geoinformation 67: 54-68. doi: 10.1016/j.jag.2018.01.001

Emre Ö, Duman TY, Özalp S, Elmacı H, Olgun Ş et al. (2013). Active Fault Map of Turkey with and Explanatory Text, General Directorate of Mineral Research and Exploration, Special Publication Series 30, Ankara, Turkey.

Farr TG, Rosen PA, Caro E, Crippen R, Duren R et al. (2007). The shuttle radar topography mission. Reviews of Geophysics: 45 (2). doi: 10.1029/2005RG000183

Fernandez J, Prieto JF, Escayo J, Camacho AG, Luzón F et al. (2018). Modeling the two-and three-dimensional displacement field in Lorca, Spain, subsidence and the global implications. Scientific reports 8 (1): 1-14. doi: 10.1038/s41598-018-33128-0

Ferretti A, Prati C, Rocca F (2001). Permanent Scatterers in SAR Interferometry. EEE Transactions on Geoscience and Remote Sensing 39 (1): 8-20. doi: 10.1109/36.898661

Figueroa-Miranda S, Tuxpan-Vargas J, Ramos-Leal JA, Hernández-Madrigal VM, Villaseñor-Reyes CI (2018). Land subsidence by groundwater over-exploitation from aquifers in tectonic valleys of Central Mexico: A review. Engineering Geology 246: 91-106. doi: 10.1016/j.enggeo.2018.09.023

Gabriel A K, Goldstein RM, Zebker H A (1989). Mapping small elevation changes over large areas: differential radar interferometry. Journal of Geophysical Research: Solid Earth 94 (B7): 9183-9191. doi: 10.1029/JB094iB07p09183.

Haghighi MH, Motagh M (2018). Ground surface response to continuous compaction of aquifer system in Tehran, Iran: Results from a long- term multi-sensor InSAR analysis. Remote Sensing of Environment 221: 534-550. doi: 10.1016/j.rse.2018.11.003

Hakyemez HY, Elibol E, Umut M, Bakırhan B, Dağıstan H et al. (1992). Geology of the Çumra Akören (Konya). MTA Report 9449, pp. 63, Ankara.

Hooper A (2008). A Multi-temporal InSAR method incorporating both persistent scatterer and small baseline approaches. Geophysical Research Letters 35(16). doi: 10.1029/2008GL034654

Hooper A, Bekaert D, Spaans K, Arıkan M (2011). Recent advances in SAR interferometry time series analysis for measuring crustal deformation. Tectonics 514-517: 1-13. doi: 10.1016/j.tecto.2011.10.013

Imamoglu M, Kahraman F, Cakir Z, Sanli FB (2019). Ground deformation analysis of Bolvadin (W. Turkey) by means of multi-temporal InSAR techniques and Sentinel-1 data. Remote Sensing 11(9): 1069. doi: 10.3390/rs11091069

Kampes B, Stefania, U (1999). The Delft Object-Oriented Radar Interferometric Software. In: The 2nd International Symposium on Operationalization of Remote Sensing, Enschede; Netherlands. pp. 16.

Khorrami M, Abrishami S, Maghsoudi Y, Alizadeh B, Perissin D (2020). Extreme subsidence in a populated city (Mashhad) detected by PSInSAR considering groundwater withdrawal and geotechnical properties. Scientific Reports 10 (1): 1-16. doi: 10.1038/s41598-020-67989-1

Koçyiğit A, Ünay E, Saraç G (2000). Episodic graben formation and extensional neotectonic regime in west central Anatolia and Isparta Angle; a case study in the Akşehir-Afyon graben, Turkey, in Tectonics and magmatism in Turkey and surrounding area. In: Bozkurt E, Winchester JA, Piper JDA (editors). Special Publication, London: Geological Society, pp 405–421.

Maerten F, Resor P, Pollard D, Maerten L (2005). Inverting for Slip on Three-Dimensional Fault Surfaces Using Angular Dislocations. Bulletin of the Seismological Society of America 95 (5): 1654-1665. doi: 10.1785/0120030181

Motagh M, Shamshiri R, Haghighi MH, Wetzel HU, Akbari B et al. (2017). Quantifying groundwater exploitation induced subsidence in the Rafsanjan plain, southeastern Iran, using InSAR time- series and in situ measurements. Engineering Geology 218: 134–151. doi: 10.1016/j.enggeo.2017.01.011

Motagh M, Walter TR, Sharifi MA, Fielding E, Schenk A et al. (2008). Land subsidence in Iran caused by widespread water reservoir

overexploitation. Geophysical Research Letters 35 (16): doi: 10.1029/2008GL033814

Okada Y (1985). Surface deformation due to shear and tensile faults in a half-space. Bulletin of the Seismological Society of America 75 (4): 1135-1154.

Orhan O (2021). Monitoring of land subsidence due to excessive groundwater extraction using small baseline subset technique in Konya, Turkey. Environmental Monitoring and Assessment 193 (4): 1-17. doi: 10.1007/s10661-021-08962-x

Orhan, O, Oliver-Cabrera, T, Wdowinski, S, Yalvac, S, Yakar, M (2021). Land subsidence and its relations with sinkhole activity in Karapınar region, Turkey: a multi-sensor InSAR time series study. Sensors 21 (3) : 774.

Peduto D, Cascini L, Arena L, Ferlisi S, Fornaro G et al. (2015). A general framework and related procedures for multiscale analyses of DInSAR data in subsiding urban areas. ISPRS Journal of Photogrammetry and Remote Sensing 105: 186-210. doi: 10.1016/j.isprsjprs.2015.04.001

Riel B, Simons M, Ponti D, Agram P, Jolivet R (2018). Quantifying ground deformation in the Los Angeles and Santa Ana Coastal Basins due to groundwater withdrawal. Water Resources Research 54 (5): 3557-3582. doi: 10.1029/2017WR021978

Rosen PA, Hensley S, Joughin IR, Li FK, Madsen SN et al. (2000). Synthetic aperture radar interferometry. Institute of Electrical and Electronics Engineers 88 (3): 333–382. doi: 10.1109/5.838084

Rosi A, Tofani V, Agostini A, Tanteri L, Stefanelli CT et al. (2016). Subsidence mapping at regional scale using persistent scatters interferometry (PSI): The case of Tuscany region (Italy). International Journal of Applied Earth Observation and Geoinformation 52: 328-337. doi: 10.1016/j.jag.2016.07.003

Sandwell D, Mellors R, Tong X, Wei M, Wessel P (2011) Open Radar Interferometry Software for Mapping Surface Deformation. Eos, Transactions American Geophysical Union 92 (28): 234. doi: 10.1029/2011EO280002

Şengör AMC (1980). Principles of neotectonics of Turkey. In: Geological Society of Turkey Conference Series 2, pp. 40, Ankara.

Şengör AMC, Yılmaz Y (1981). Tethyan evolution of Turkey: A plate tectonic approach. Tectonophysics 75: 181-241.

Thomas AL (1993). Poly3D: a three-dimensional, polygonal element, displacement discontinuity boundary element computer program with applications to fractures, faults, and cavities in the earth's crust. M.S. Thesis, Stanford University, Stanford, California, 221p

Ustun A, Tusat E, Yalvac S (2010). Preliminary results of land subsidence monitoring project in Konya Closed Basin between 2006–2009 by means of GNSS observations. Natural Hazards and Earth System Sciences 10 (6): 1151-1157. doi: 10.5194/nhess-10-1151-2010

Ustun A, Tuşat E, Yalvaç S, Özkan İ, Eren Y, Özdemir A, Bildirici İÖ, Üstüntaş T, Kırtıloğlu OS, Mesutoğlu M (2015). Land subsidence in Konya Closed Basin and its spatio-temporal detection by GPS and DInSAR. Environ. Earth Science 73:6691–6703. doi: 10.1007/s12665-014-3890-5